Limited Role of Absolute Humidity in Intraurban Heat Variability

DARRYN W. WAUGH^O, BENJAMIN ZAITCHIK, ANNA A. SCOTT, PETER C. IBSEN, G. DARREL JENERETTE, JASON SCHATZ, AND CHRISTOPHER J. KUCHARIK^{e,f}

- a Department of Earth and Planetary Sciences, The Johns Hopkins University, Baltimore, Maryland
- b Geosciences and Environmental Change Science Center, U.S. Geological Survey, Denver, Colorado
- ^c Department of Botany and Plant Sciences, University of California, Riverside, Riverside, California

 ^d SkyTruth, Santa Fe, New Mexico

(Manuscript received 5 June 2023, in final form 26 October 2023, accepted 30 October 2023)

ABSTRACT: Monitoring and understanding the variability of heat within cities is important for urban planning and public health, and the number of studies measuring intraurban temperature variability is growing. Recognizing that the physiological effects of heat depend on humidity as well as temperature, measurement campaigns have included measurements of relative humidity alongside temperature. However, the role the spatial structure in humidity, independent from temperature, plays in intraurban heat variability is unknown. Here we use summer temperature and humidity from networks of stationary sensors in multiple cities in the United States to show spatial variations in the absolute humidity within these cities are weak. This variability in absolute humidity plays an insignificant role in the spatial variability of the heat index and humidity index (humidex), and the spatial variability of the heat metrics is dominated by temperature variability. Thus, results from previous studies that considered only intraurban variability in temperature will carry over to intraurban heat variability. Also, this suggests increases in humidity from green infrastructure interventions designed to reduce temperature will be minimal. In addition, a network of sensors that only measures temperature is sufficient to quantify the spatial variability of heat across these cities when combined with humidity measured at a single location, allowing for lower-cost heat monitoring networks.

SIGNIFICANCE STATEMENT: Monitoring the variability of heat within cities is important for urban planning and public health. While the physiological effects of heat depend on temperature and humidity, it is shown that there are only weak spatial variations in the absolute humidity within nine U.S. cities, and the spatial variability of heat metrics is dominated by temperature variability. This suggests increases in humidity will be minimal resulting from green infrastructure interventions designed to reduce temperature. It also means a network of sensors that only measure temperature is sufficient to quantify the spatial variability of heat across these cities when combined with humidity measured at a single location.

KEYWORDS: Humidity; Health; Heat islands; Urban meteorology

1. Introduction

As the frequency of extreme events has risen in recent decades (Seneviratne et al. 2021) and appreciation of urban vulnerability to heat events has increased (e.g., Hoffman et al. 2020; Tuholske et al. 2021), city governments and their partners have prioritized high-resolution heat vulnerability analysis (e.g., Scott et al. 2017; Shandas et al. 2019; Saverino et al. 2021). This has led to a growth in the number of studies measuring heat microclimates within cities, either with fixed location networks (e.g., Yang et al. 2013; Schatz and Kucharik 2014; Scott et al. 2017; Fenner et al. 2019; Richard et al. 2021; Ibsen et al. 2021) or mobile networks (e.g., Shandas et al. 2019; Ziter et al. 2019; Alonzo et al. 2021). These studies have quantified a wide range of aspects of urban heat variability, including how this variability changes during hot weather extremes, and its dependence on the characteristics of the urban

Corresponding author: Darryn Waugh, waugh@jhu.edu

landscape (e.g., percentage impervious surfaces, green space, tree canopy cover). However, although motivated by the health impacts of urban heat, the majority of these studies have focused only on the spatial variability of air temperature T, and it is widely recognized that T alone does not sufficiently describe conditions that can lead to physiological heat stress (e.g., Taleghani et al. 2016).

When quantifying ambient environmental conditions relevant to heat exposure, it is important to consider some combination of temperature, humidity, radiation, and wind, all of which contribute to the rate at which an exposed individual is externally heated and is able to dissipate heat. To account for these conditions, a number of different heat metrics have been proposed, including wet-bulb globe temperature (e.g., Budd 2008), apparent temperature (e.g., Steadman 1984), heat index (e.g., Anderson et al. 2013; Lu and Romps 2022), and humidity index (humidex; e.g., Gosling et al. 2014), and universal thermal climate index (Błażejczyk et al. 2013).

While these metrics are more predictive of health impacts than temperature alone, they are difficult to calculate using

^e Nelson Institute Center for Sustainability and the Global Environment, University of Wisconsin-Madison, Madison, Wisconsin Department of Agronomy, University of Wisconsin-Madison, Madison, Wisconsin

the low-cost instruments frequently employed in urban heat mapping campaigns. There is a trade-off between the spacetime resolution that a monitoring network can achieve and the number of variables that can be measured within a limited budget.

Here, we focus on the spatial variability in absolute humidity within a city. We do this because humidity is a critical input to almost all proposed physiologically relevant heat metrics, it is the sole input (other than T) for widely used indices such as the heat index (HI) and the humidex (Hx), and humidity is measured by networks in several cities. Also, few studies have quantified the intraurban variation of absolute humidity. One exception is Hall et al. (2016) who examined variations in T and absolute humidity in six cities in the United States. They showed the microclimate of residential yards were more similar between cities than native landscapes. However, they had limited sampling within urban environments and did not quantify the role variations in absolute humidity [as opposed to temperature, which has a strong control on relative humidity (RH)] played in the spatial variability of heat within cities. This is the central goal of this study.

A similar question can also be asked about the role of absolute humidity in spatial variations of vapor pressure deficit (VPD). The VPD is the difference between the saturation water vapor pressure and the actual water vapor pressure and is closely connected to plant transpiration/atmospheric water demand for plants (e.g., Farquhar and Sharkey 1982; Grossiord et al. 2020; Novick et al. 2016). The VPD depends on both T and absolute humidity, and as with the heat indices there have been limited studies of the relative role of these factors in driving variations in VPD. An exception is Zipper et al. (2017), who showed that the urban–rural difference in VPD in Madison, Wisconsin, is almost entirely driven by temperature variations.

In this study, we quantify the spatial variability of absolute humidity within multiple cities and the role this plays in the spatial variability of heat indices. This is fundamental for understanding intraurban heat variability and is also relevant for assessing the effectiveness of interventions designed to reduce temperature—most notably, green infrastructure interventions, which might be expected to increase absolute humidity. If this increase in humidity is substantial, the effectiveness of green infrastructure for heat reduction will be smaller than what is reported based on temperature reductions alone.

A more practical reason to quantify the spatial variability of absolute humidity is that if this variability is small, then spatially distributed measurements of T alone (with humidity measured at a single location) will be sufficient to estimate the spatial variability of HI: that is, the RH and HI could be estimated at each location and time using the local T measurement and the single humidity measurement obtained from a central monitoring site, such as a synoptic weather station. This is relevant because sensors that measure both T and RH have a significantly higher price point than sensors that measure T alone. The same approach could also be used in cases where there are maps showing spatial distribution of T (from, e.g., a statistical land-use regression model) but not RH.

Here, we quantify the spatial variability of summertime water vapor mixing ratio w in nine cities in the United States, using hourly measurements of T and RH from networks of fixed sensors in these cities. We quantify the spatial variations in humidity and estimate its impact on variations in heat metrics (HI and Hx) and VPD. The cities sampled are of different sizes and climates (including humid coast and hot desert climates), and comparison of the cities provides insights in the robustness/generalizability of the results. Different instrumentations were used among some of the cities, and this again provides insight into the robustness of results, especially in cities where we are able to validate results from multiple deployments using different instrumentation.

The data and methods used are described in the next section. In section 3 we analyze the equations for HI and Hx to quantify the sensitivity of RH, HI, Hx, and VPD to variations in w or T, to help interpretation of the observations. The data from Baltimore, Maryland, and other cities are then analyzed in sections 4a and 4b, respectively. Concluding remarks are in section 5.

2. Data and methods

a. Data

We use T and RH data from sensor networks deployed by research groups at three different universities: The Johns Hopkins University (JHU), University of California Riverside (UCR), and University of Wisconsin-Madison (UWM).

The JHU measurements were made in Baltimore in summer 2016 and 2017 (Shi et al. 2021). These networks consist of Maxim Integrated Products, Inc., "iButton" Model DS1923 thermometer/hygrometers, with a temperature accuracy of ±0.58C from 108 to 658C and RH accuracy of ±0.5% from 0% to 100%. These sensors were placed inside a custom radiation shield (Zaitchik et al. 2016) in trees. [Note that for the 2016 deployment, as in the 2015 deployment described in Scott et al. (2017), the sensors were placed on poles or trees, but here we use only sensors that were in trees.] Although all sensors were placed in trees, the trees are located in a wide range of local environments, including on streets, within parks, and in urban forests, and are distributed across the city (Fig. 1). Trees reduce the amount of direct radiation on placed sensors, which reduces the bias inherent in many purchased or novel-designed shielding (Terando et al. 2017). The number and location of the sensors varied between years, with 57 within Baltimore City in 2016 and 55 in 2017 (with 19 at the same locations in both summers). We examine hourly measurements of T and RH between 15 July and 31 August for 2016 and 2017.

The UCR measurements were made in eight different cities, including Baltimore (see Table 1). This network used the same iButton DS1923 sensors, inside a custom radiation shield, and placed on trees (Ibsen et al. 2021). The radiation shield used was of a different design from that used in the JHU deployments [see Fig. 1d of Ibsen et al. (2021)]. Locations of sensor deployment were determined by randomly selecting locations within five binned categories of normalized

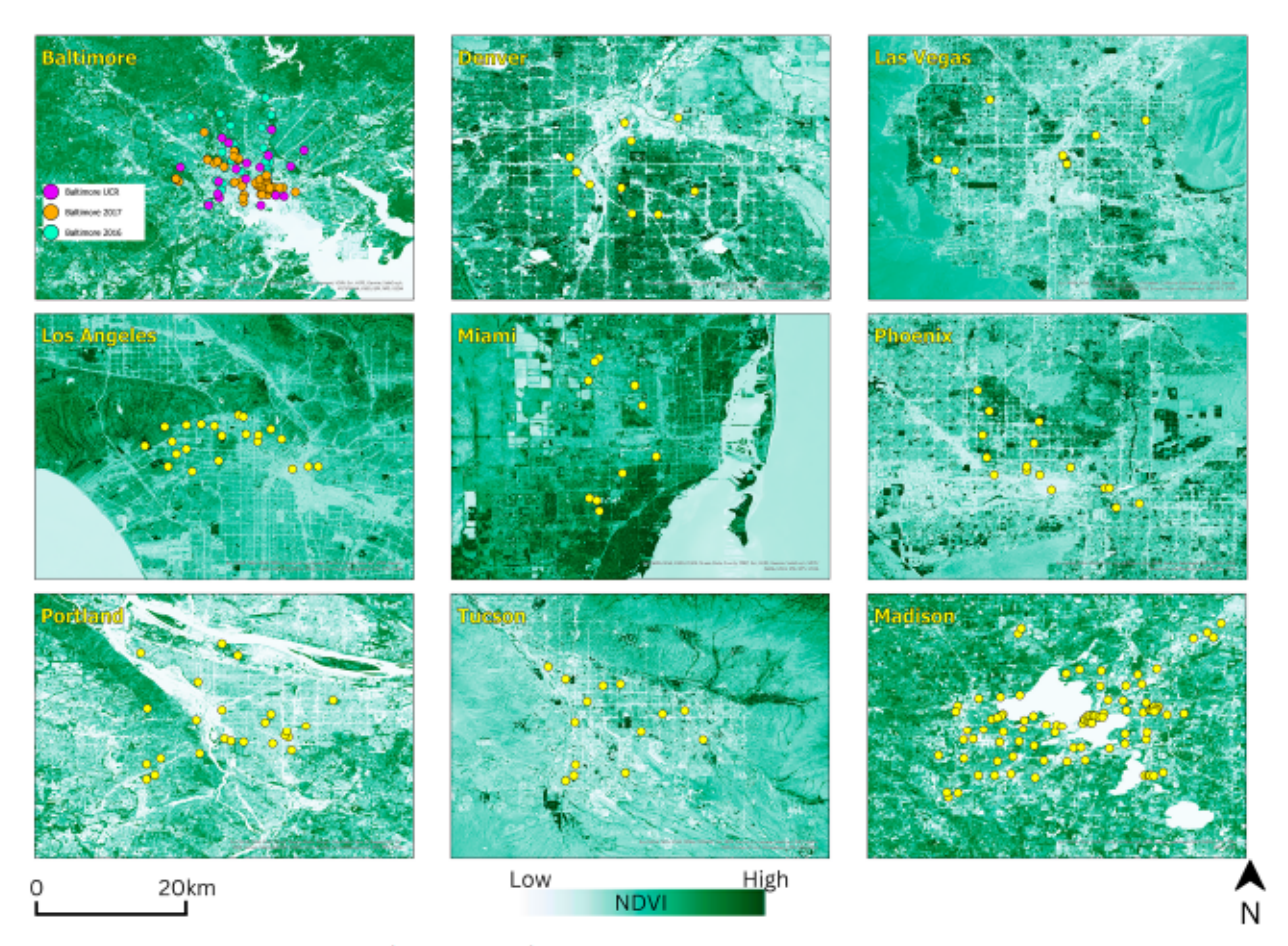


FIG. 1. Maps of the Sentinel-2 L1C data (Phiri et al. 2020). A median composite for June–August 2022 was created in Google Earth Engine, as derived from Copernicus Sentinel data (Copernicus 2023).

difference vegetation index (NDVI) values spanning the range within each city [see Ibsen et al. (2021) for details]. Hence, as with the JHU network, these measurements were made in a wide range of local environments. The number of sensors, year, and time of deployment varied by city, see Table 1 and Fig. 1. The numbers of sensors for each of the UCR deployments listed in Table 1 are much smaller than

those listed in Ibsen et al. (2021) as most of the iButton sensors used in the deployments measure only temperature [the focus of Ibsen et al. (2021)], and not T and RH. In addition, for Tucson, Arizona; Las Vegas, Nevada; and Phoenix, Arizona we have removed 1-3 sensors whose measurements are outliers (in some cases these appear to be due to irrigation in the morning, with RH spiking to 100% for 1-2 h).

TABLE 1. Information for each study city: Institution that collected the data, the mean (with standard deviation in parentheses) of the deployment-mean temperature T and water vapor mixing ratio w, the number of sensors N, and the period that was analyzed. The values for Madison are an average of the multiple years.

City	Group	T at 1500 LT (8C)	w at 1500 LT (g kg ⁻¹)	N	Dates
Baltimore, Maryland (BAL)	JHU	31.1 (1.3)	15.1 (0.4)	57	15 Jul-31 Aug 2016
BAL	JHU	28.1 (1.1)	14.0 (0.4)	55	15 Jul-31 Aug 2017
BAL	UCR	28.4 (1.0)	13.1 (0.2)	18	11 Jul-30 Sep 2017
Denver, Colorado (DEN)	UCR	30.6 (1.1)	7.9 (0.4)	10	10 Jul-12 Sep 2018
Las Vegas, Nevada (LAS)	UCR	40.4 (1.9)	7.2 (0.2)	7	11 Jun-19 Aug 2018
Los Angeles, California (LOS)	UCR	29.0 (1.4)	12.8 (0.3)	22	23 Jun-14 Sep 2017
Miami, Florida (MIA)	UCR	31.9 (0.6)	18.9 (0.3)	10	1 Jul-17 Sep 2018
Phoenix, Arizona (PHX)	UCR	42.1 (1.8)	10.0 (0.4)	16	15 Jun-15 Aug 2017
Portland, Oregon (PTL)	UCR	28.3 (1.8)	9.4 (0.3)	25	20 Jun-24 Aug 2017
Tucson, Arizona (TUC)	UCR	40.4 (1.0)	8.8 (0.3)	14	14 Jun-7 Sep 2019
Madison, Wisconsin (MSN)	UWM	26.0 (0.4)	12.9 (0.3)	90	15 Jul-31 Aug 2012-19

We examine the hourly data for the different periods of each city's deployment.

The UWM network is in Madison (Schatz and Kucharik 2014, 2015), and measurements have been made since 2012. This network consists of HOBO U23 Pro v2 temperature/RH dataloggers in solar radiation shields from Onset Computing installed on streetlight and utility poles across the Madison area [Fig. 1 of Schatz and Kucharik (2014)]. Sensor accuracy is 0.218C from 08 to 508C for dry-bulb temperature and 2.5% from 10% to 90% for humidity. Measurements have been available since 2012. We select the sensors identified in the dataset as urban (whose number varied between 83 and 93 for different years) and examine the same period of 15 July–31 August as the Baltimore data for years between 2012 and 2019.

b. Analysis methods

From the hourly measurements of T and RH we calculate different measures of humidity and heat. We calculate the vapor pressure $e = e_s \times RH$, where e_s is the saturation vapor pressure (hPa) (Alduchov and Eskridge 1996):

$$e_e = 6:11e^{17:625T/(2.43:04+T)}$$
, (1)

with T in degrees Celsius. We then calculate the water vapor mixing ratio w (g kg⁻¹) using w = 621.97e/(p - e), where p is atmospheric pressure (hPa), and the vapor deficit pressure VPD = $e_s - e = e_s(1 - RH)$.

In the analysis below we use the mixing ratio w as our metric of absolute humidity, but similar results are found using vapor pressure or dewpoint temperature Td. For simplicity, we use global-mean sea level pressure p=1013.25 hPa in the calculation of w. This results in an underestimate of the mixing ratio for higher elevation cities that have lower p (e.g., Denver, Colorado). This bias will apply for all stations at each city and, while it could impact comparison of absolute values between cities, it does not impact our analysis of variations within cities. Also, the use of the same p for all cities makes easier comparison of values among cities, and means the vapor pressure can be easily estimated from values of w reported below [i.e., because $e \ll p$, $e \sim (p/621.97)w = 1.63w$, for w in grams per kilogram and e in hectopascals].

For heat, we calculate two commonly used metrics that only depend on T and RH: HI, which is commonly used in the United States, and Hx, which is used by Environment Canada. Many formulas have been used to calculate HI [see Anderson et al. (2013) for comparisons], and here we use the U.S. National Weather Service method. This is not a single equation but rather an algorithm involving several steps and decision points, which is documented in Fig. 3 of Anderson et al. (2013). Lu and Romps (2022) recently updated the HI calculation and extended it to higher T and RH, but for the range of T and RH that occur in cities studied here the differences between their method and that used by U.S. National Weather Service are small.

The Hx is calculated as (Gosling et al. 2014)

$$Hx = T + \frac{5}{9}(6:11 \exp\{5417:753[(1/273:16) - (1/T_d)]\} - 10),$$

where T, Td, and Hx are all in degrees Celsius. To allow easier comparison with HI, we re-express Hx in degrees Fahrenheit (the magnitude of a degree Celsius is 5/9 of a degree Fahrenheit, and there is an additive offset involved in the conversion from Celsius to Fahrenheit).

To quantify the role spatial variability in w plays in the variability in the heat metrics, we estimate RH, HI, and Hx at each location using the T at that location together with w averaged over all sites (which we refer to as the spatial-mean mixing ratio \overline{w}). The spatial variability in these estimates (referred to as RH*, HI*, and Hx*) is due only to variability in T, and the difference between these estimates and the observed spatial variability is due to spatial variability in w. The difference is quantified by calculating the root-mean-square error between RH* and RH [referred to as RMSE(RH*)], and by comparing the spatial standard deviation of RH* and RH [i.e., comparing σ (RH*) and σ (RH)]. The calculation of RH*, VPD*, HI*, and Hx* is done for summer-mean values as well as for the hourly data.

3. Heat index dependence on humidity

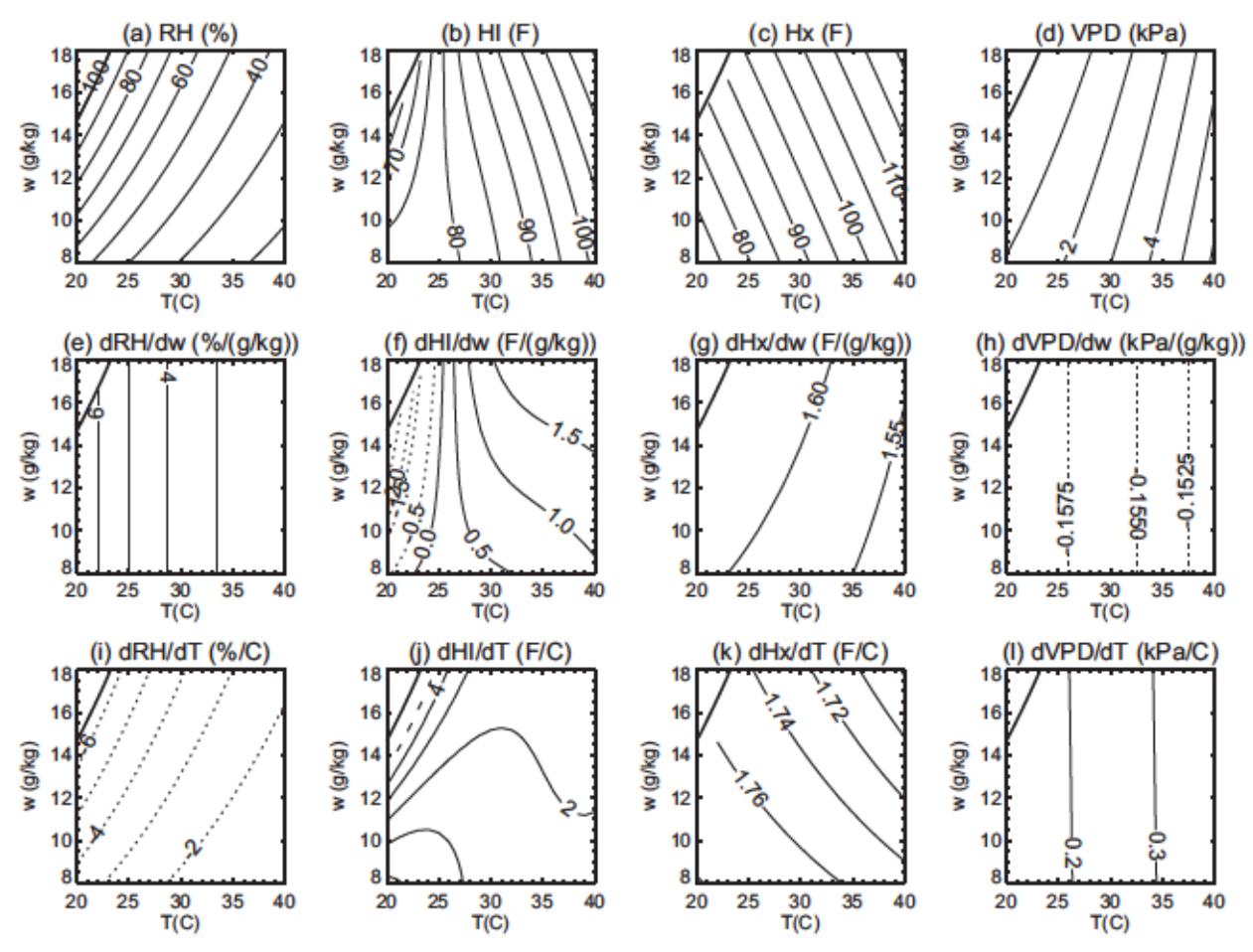
Before we perform an analysis of the observed T and RH, we analyze the equations for the different metrics to quantify the sensitivity of each field to T and w. The change (in time or space) of a field X (e.g., RH, HI, Hx, or VPD) that depends on T and w can be approximated as

$$\Delta X \approx \frac{\partial X}{\partial w} \Delta w + \frac{\partial X}{\partial T} \Delta T,$$
 (3)

where the partial derivatives $\partial X/\partial w$ and $\partial X/\partial T$ are a measure of the sensitivity of X to changes in w and T. Quantifying these sensitivities will help in the interpretation of the data presented in the following sections, and it will also be useful for considering the impact of w in other cities.

The variation of RH, HI, Hx, and VPD together with their sensitivities, with T and w are shown in Fig. 2. As is well known, RH increases with w but decreases with T (Fig. 2a), which corresponds to $\partial RH/\partial w > 0$ (Fig. 2e) and $\partial RH/\partial T < 0$ (Fig. 2i). Although the sign of the sensitivity of RH to w and T differs the magnitudes are similar, that is, $\partial RH\partial w \sim 2\%-6\%$ (g kg⁻¹)⁻¹ and $\partial RH\partial T$ goes from -2% to -6% $\& C^{-1}$, with larger values for lower T. This means that the change in RH due to w and T [i.e., the two terms on the right-hand side of Eq. (3)] will be similar, if the change in w and T are of similar magnitude for w in grams per kilogram and T in degrees Celsius.

The sensitivities of HI, Hx, and VPD to w and T are also of similar magnitude, for example, for $T \sim 30 \, \text{RC}$, $\partial \text{HI}/\partial w \sim 18 \, \text{F} \, (\text{g kg}^{-1})^{-1}$ and $\partial \text{HI}/\partial T \sim 28 \, \text{F} \, 8 \, \text{C}^{-1}$ (Figs. $2 \, \text{g.j.}$); $\partial \text{Hx}/\partial w \sim 1.68 \, \text{F} \, (\text{g kg}^{-1})^{-1}$ and $\partial \text{Hx}/\partial T \sim 1.75 \, \text{F} \, 8 \, \text{C}^{-1}$ (Figs. $2 \, \text{g.k.}$); and $\partial \text{VPD}/\partial w \sim 0.15 \, \text{kPa} \, (\text{g kg}^{-1})^{-1}$ and $\partial \text{VPD}/\partial T \sim 0.25 \, \text{F} \, 8 \, \text{C}^{-1}$ (Figs. $2 \, \text{h.J.}$). Thus, for all metrics the changes due to w and T will be similar if the variations in w and T are similar (again for w in grams per kilogram and T in degrees Celsius). In other words, if the spatial variance of w and T are similar within a city, then changes in both will impact the spatial variance of RH, VPD,



Ftg. 2. Variation with T and w of (a) RH (%), (b) HI (8F), (c) Hx (8F), and (d) VPD (kPa); partial derivatives of (e) RH, (f) HI, (g) Hx, and (h) VPF with respect to w; and partial derivatives of (i) RH, (j) HI, (k) Hx, and (l) VPD with respect to T. The thick line shows RH = 100%, and values are not plotted for RH > 100%.

HI, and Hx, but if the variance in w is much less than the variance in T, then variations in w may not play a major role in intraurban variance of HI and Hx. As we show below, the latter is the case for all cities studied.

4. Results

a. Baltimore

We first consider the spatial variation of *T*, *w* and other fields in Baltimore. We focus first on summer-mean (15 July-31 August) values of measurements made in 2016. All fields show a range of values across the city, both in the morning and afternoon, see Fig. 3. The spatial variations in *T*, RH, VPD, and the heat metrics are highly correlated or anticorrelated, with lower RH and higher VPD, HI, and Hx when higher *T* (in both the morning and afternoon). This can be seen in Fig. 3, which shows the values of the summer-mean *w* (Fig. 3a), RH (Fig. 3b), VPD (Fig. 3c), HI (Fig. 3d), and Hx (Fig. 3e) at 0600 and 1500 local time (LT), plotted against the summer-mean *T*. The magnitude of the linear correlation coefficient *r* between *T* and RH, VPD, HI, or Hx exceeds 0.95.

The situation is, however, different for w: correlations are insignificant between w and T in the morning (e.g., $r \sim 0.15$ at 0600 LT) and there are only moderate anticorrelations in the afternoon (e.g., r = -0.65 at 1500 LT) (Fig. 3a). The weaker w-T relationships in comparison with the high correlations of the other fields with T suggests that the spatial variability of these fields is dominated by variations in T, with a smaller role from w.

A possible cause for the afternoon correlation could be the impact of vegetation on both humidity and temperature. Vegetation amount, determined using NDVI, and summer-mean T are significantly negatively correlated for all hours (with correlation coefficient r from approximately -0.6 to -0.8). This is consistent with lower temperatures due to increased shade and latent heat fluxes. NDVI and w in the afternoon ($r \sim 0.7$) show significant positive correlation but insignificant in the morning ($r \sim 0.2$). The positive correlation with NDVI in the afternoon but not overnight to the morning is consistent with increased daytime transpiration at more vegetated sites. The negative T correlation with NDVI and positive w correlation with NDVI during the afternoon results in the moderate w-T anticorrelation in the afternoon.

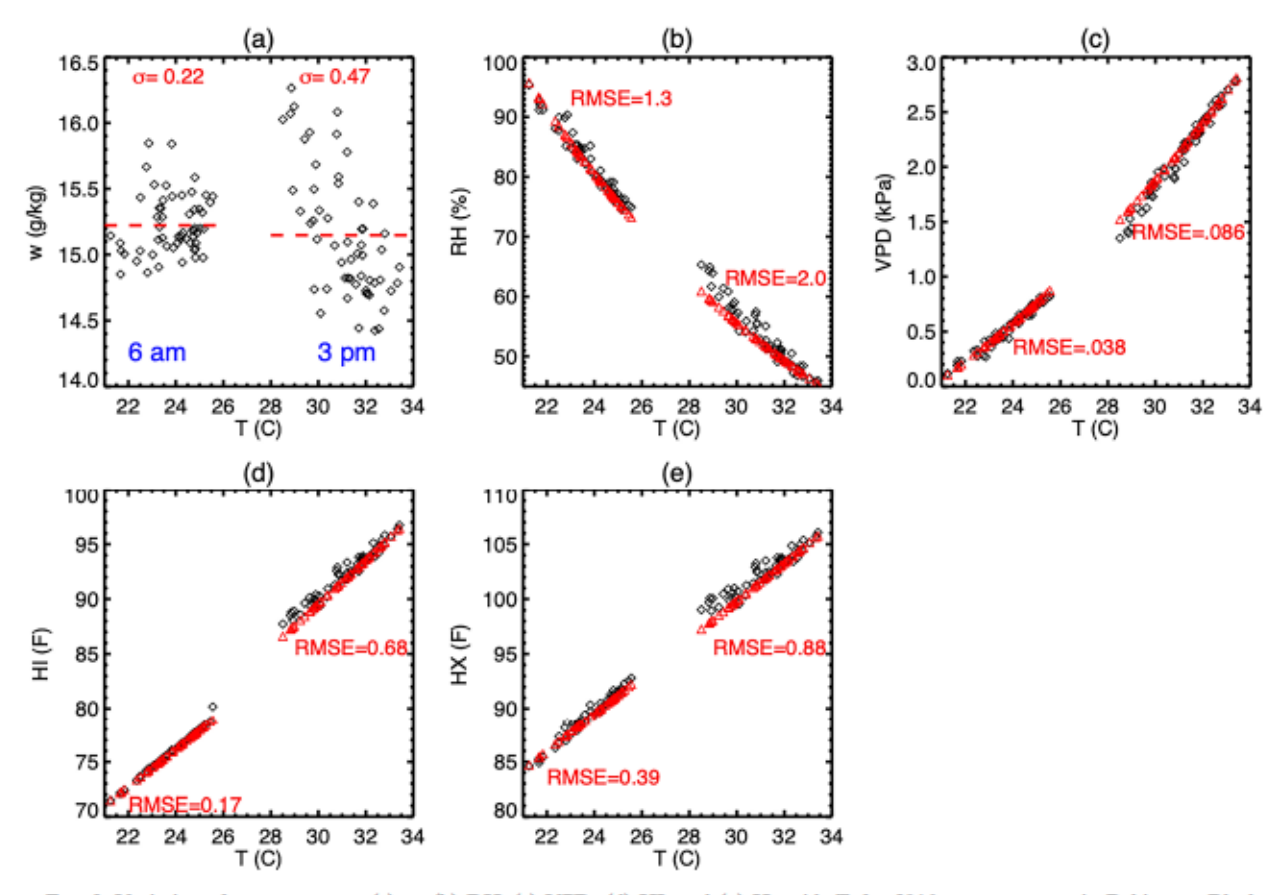


FIG. 3. Variation of summer-mean (a) w, (b) RH, (c) VPD, (d) HI, and (e) Hx with T, for 2016 measurements in Baltimore. Black symbols show the true measured values, red dashed lines in (a) show \overline{w} , and red symbols in (b)–(e) show the estimates RH*, VPD*, HI*, and Hx*. The points with T < 288C correspond to 0600 LT data, and those with T > 288C correspond to 1500 LT data.

The diurnal cycle of w also differs from those of RH, VPD, HI, and Hx. The spatial variances of RH, HI, and Hx (as well as T) are similar in the morning and afternoon, and the differences between the spatial-mean in the morning and afternoon are larger than the range at either time, resulting in a separation between morning and evening values (Figs. 3b-e). In contrast, diurnal cycle is limited in the spatial-mean w and spatial variance is larger in the afternoon than in the morning, resulting in an overlap of the morning and afternoon distributions of w (Fig. 3a). The difference between morning and afternoon values of RH, VPD, HI, and Hx even though w is similar in the morning and afternoon suggests that variations in T also dominate the diurnal variation of RH, HI, and Hx.

While the above suggests that T variations dominate the variability in HI and Hx, it does not provide an estimate of the magnitude of the impact of w variations. Such an estimate can be obtained using the observed spatial standard deviations of w and T, the HI and Hx sensitivities from section 3 (Fig. 3), and Eq. (3). At 1500 LT, the observed standard deviations are $\sigma(w) \sim 0.5 \text{ g kg}^{-1}$ and $\sigma(T) \sim 1.38\text{F}$. Combining these with sensitivities $d\text{HI}/dw \sim 1.08\text{F} (\text{g kg}^{-1})^{-1}$ and $d\text{HI}/dT \sim 28\text{F 8C}^{-1}$ indicates that variations in w will lead to $\sigma(\text{HI}) \sim 0.5 \text{ g kg}^{-1} \times 1.08\text{F} (\text{g kg}^{-1})^{-1} = 0.58\text{F}$ while variations in T will lead to higher $\sigma(\text{HI}) \sim 1.3 \times 2 = 2.68\text{F}$. For 0600 LT, the difference is

even larger, the estimated change in $\sigma(HI)$ due to w is only $\sim 0.2 \times 0.2 = 0.048F$ as compared with $\sim 1.1 \times 1.75 = 28F$ due to T variations. Similar results hold for VPD and Hx, and this analysis indicates that variations in w play a minor role in the spatial variations of the heat metrics, especially in the morning.

To quantify the contributions of T and w more precisely we use, as described in section 2, the spatial-mean \overline{w} rather than the actual w together with T at each site to estimate RH, HI, and Hx at each site, that is, calculate $RH_i^{\bullet} = RH(T_i, \overline{w})$ at each site i. For all fields, the estimated values are close to the true values, see red symbols in Figs. 3b-e. The RMSE between RH* and RH is only 1.3% at 0600 LT and 2% at 1500 LT, and the RMSE for HI* and Hx* are 0.178 and 0.398F at 0600 LT, respectively, and 0.68 and 0.88 at 1500 LT Consistent with the larger variability in afternoon w, the errors are larger in the afternoon (see also Fig. 4 below). However, even the afternoon RMSE are small. This indicates that the variability in w is not playing a major role in spatial variability in RH or heat indices, that is, local RH and heat metrics can be estimated using local T and the spatial-mean \overline{w} :

Analysis of all times of day shows that the RMSE are small in the morning and the largest differences occur in the afternoon (Fig. 4). Similar results are found when comparing the differences in the spatial standard deviation of the true and

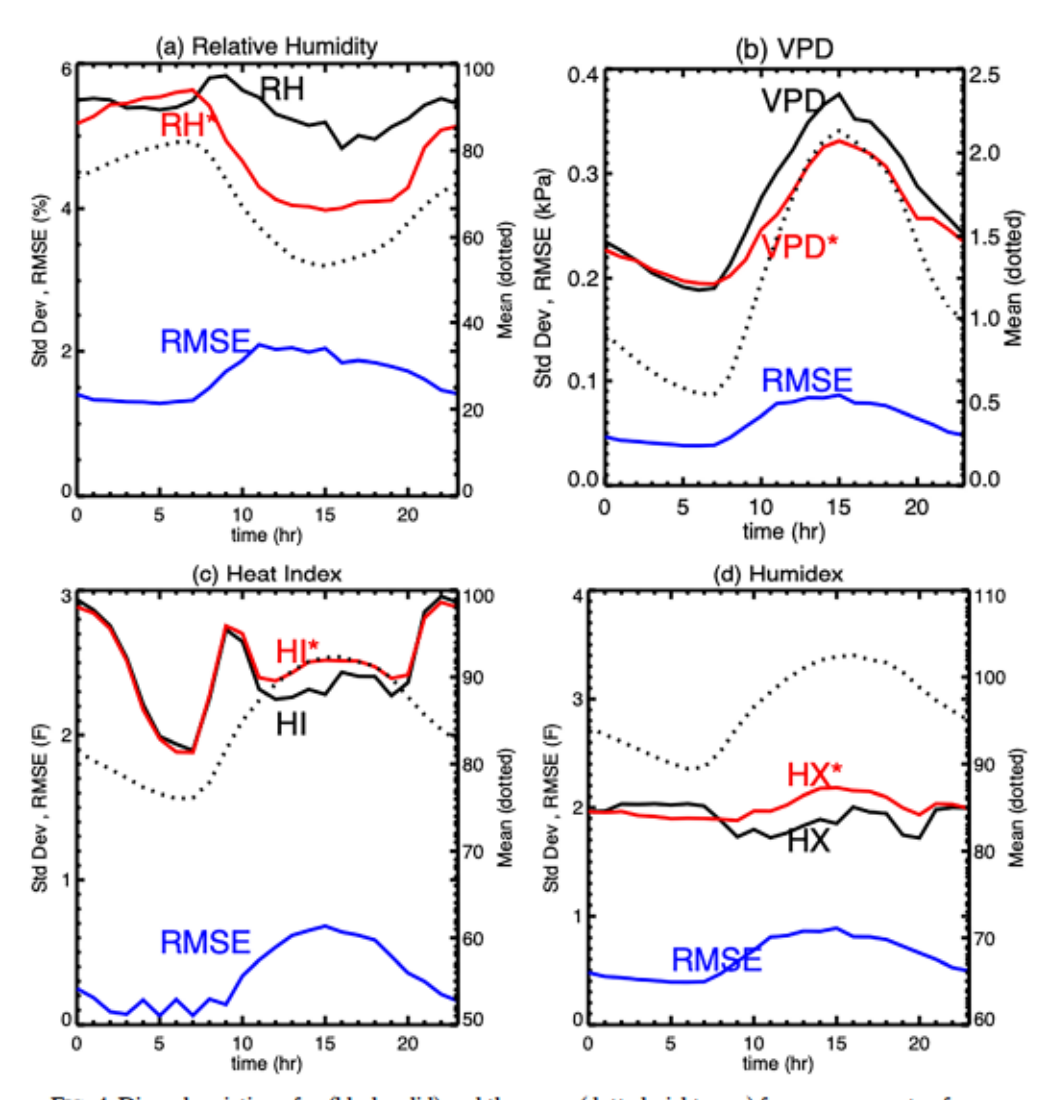


FIG. 4. Diurnal variation of σ (black solid) and the mean (dotted; right axes) for measurements of summer-mean (a) RH, (b) VPD, (c) HI, and (d) Hx. The red curves show σ of the estimates assuming uniform w, e.g., σ (RH*), and the blue curves show RMSE between true and estimated values, i.e., RMSE(RH, RH*).

estimated values, that is, comparing $\sigma(RH)$ and $\sigma(RH^*)$ in Fig. 4. There is nonnegligible difference for RH around 1500 LT, with $\sigma(RH^*) \sim 4\%$ as compared with $\sigma(RH) \sim 5\%$, but the differences for HI and Hx are still small at 1500 LT, for example, $\sigma(HI^*) \sim 2.38F$ as compared with $\sigma(HI) \sim 2.58F$. Thus, for all times of day the error in HI* and Hx* (either measured by the RMSE or in difference in σ) is small, and the spatial variance in HI and Hx can be estimated using the spatial-mean value of w.

The above analysis considered summer-mean temperature and humidity but can be repeated for individual days during the summer. The spatial variations in w are larger for daily values than summer mean but are still small ($\sigma < 1~{\rm g~kg^{-1}}$), see Fig. 5a. The errors in RH* and HI* (and Hx*) are also larger for individual hours than summer-mean, but again are still small, see Figs. 5a and 5b. In particular, the difference in $\sigma({\rm HI})$ is still only a fraction of a degree (Fig. 5c). There is relatively large day-to-day variation in spatial variance in w (with temporal standard deviation between 0.25 and 0.45 times the summer-mean), which translates in daily

variability in RMSE of RH*, HI*, and Hx* (vertical bars in Fig. 5). But even in the most extreme cases the errors in HI* and Hx* are small (less than 1.58F).

Measurements of T and RH were also made, independently, in 2017, by the JHU and UCR groups. Repeating the above analysis for each set of 2017 measurements produces similar results, for example, the spatial standard deviation of the summer-mean w is much less than that of T (Table 1), and the RMSE between the estimate indices (RH*, HI*, Hx*, and VPD*) and observed values are small, see Fig. 6. Thus, the conclusion that spatial variations in w play an insignificant role in intraurban heat variability within Baltimore holds between years and different datasets.

b. Other cities

To test whether the insignificant role of w spatial distribution holds for other cities, we repeat the above analysis for data from the other cities listed in Table 1. The cities

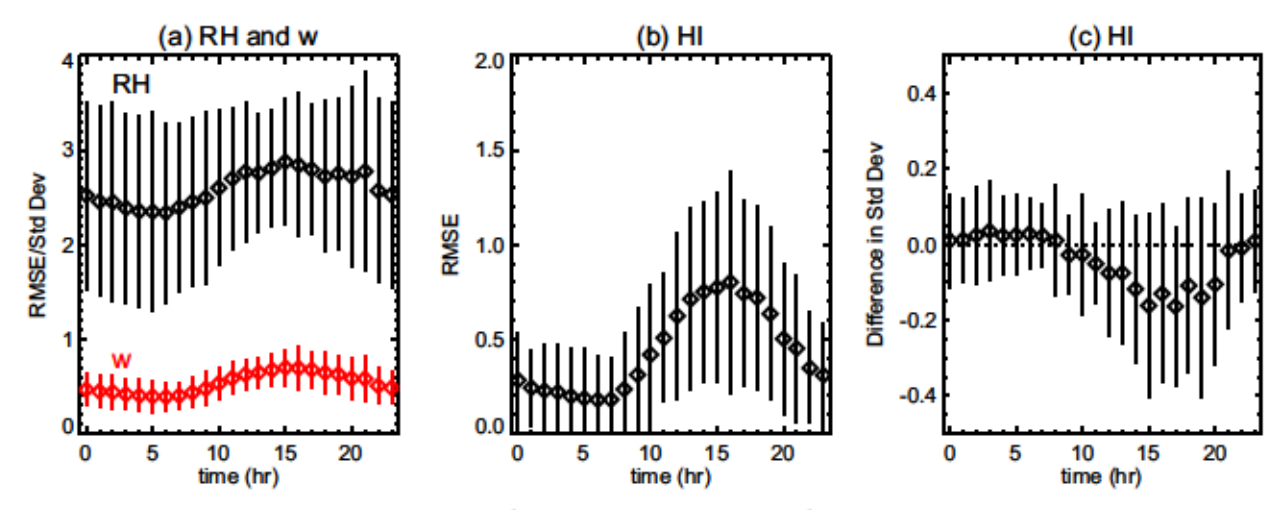


FIG. 5. Diurnal variation of (a) $\sigma(w)$ and RMSE(RH*), (b) RMSE(HI), and (c) $\sigma(HI*) - \sigma(HI)$ for hourly measurements. The symbol shows the mean value of the summer, and the vertical bar shows ± 1 temporal standard deviation.

examined have a range of climates, with spatial mean \underline{w} varying from 7 to 19 g kg⁻¹ (Table 1). However, the spatial variations of w are similar to that for Baltimore, that is, $\sigma(w) \sim 0.2-0.4$ g kg⁻¹, see Table 1 and Fig. 6.

As expected from the similar spatial variance among the cities, the RMSE between estimates assuming uniform mixing ratio (e.g., RH*) and the observed values are small, for all cities and fields considered, see Fig. 6. Specifically, RMSE(RH*) $\sim 1.5\%-2.0\%$ for morning and afternoon, RMSE(HI*) < 0.28F in the morning and $\sim 0.28-0.58F$ in the afternoon, and RMSE(Hx*) < 0.38-0.68F in the morning and $\sim 0.58-0.88F$ in the afternoon. Although not shown in Fig. 6 RMSE is small for VPD, that is, RMSE(VPD*) $\sim 0.03-0.06$ kPa in the morning and $\sim 0.5-1.0$ kPa in the afternoon. The small error in VPD from assuming uniform w is consistent with the Zipper et al. (2017) analysis of the Madison data that showed that the urban-rural differences in VPD are almost entirely due to temperature differences rather than differences in air moisture content.

The small RMSEs shown in Fig. 6 are consistent with analysis in section 3 and Eq. (3). For example, dHI/dw < 18F (g kg⁻¹)⁻¹ and $dHx/dw \sim 1.68F$ (g kg⁻¹)⁻¹ for morning conditions in each city, coupled with observed $\sigma(w) \sim 0.2$ g kg⁻¹ suggests $\sigma(HI) < 0.28F$ and $\sigma(Hx) \sim 0.38F$, broadly consistent with Fig. 6a. For afternoon conditions, dHI/dw < 18F (g kg⁻¹)⁻¹ for some cities, but >18F (g kg⁻¹)⁻¹ for others (e.g., Phoenix; Tucson; Miami, Florida), and as a result there is a larger spread in RMSE(HI) for afternoon conditions. However, even in cities with largest RMSEs, these are a small percentage of the mean HI, that is, RMSE less than 18F for mean value around or larger than 1008F.

5. Conclusions

Measurements from networks of temperature and humidity sensors deployed in multiple cities in the United States, with different climates, show weak spatial variations in absolute

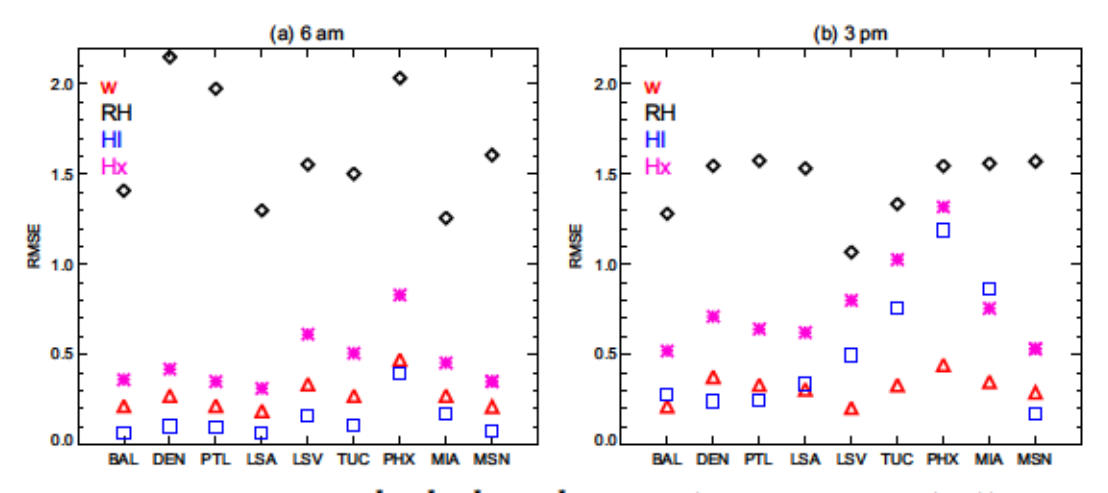


FIG. 6. RMSE for deployment-mean w*, RH*, HI*, and Hx* for each city (see Table 1 for city names) at (a) 0600 LT and (b) 1500 LT. BAL values are the UCR deployment in 2017, and values for MSN are a mean over 2012–19.

humidity during summer, for example, the spatial standard deviation of the water vapor mixing ratio, w, is around 0.2–0.4 g kg $^{-1}$, as compared with spatial-mean w values around 8–15 g kg $^{-1}$. These variations in w are much smaller than those of T, and the spatial variability in RH, VPD, and heat metrics is dominated by the variability in T. As a consequence, maps of these fields will look the same as maps of urban temperature, as Yang et al. (2017) showed for maps of RH and urban dryness. Further, results from previous studies that considered only intraurban variability in T will carry over to intraurban heat variability, and quantifying the processes that control variations in temperature is key for understanding intraurban variability.

The small spatial variability of absolute humidity within the cities indicates that the sources of humidity in urban areas are weak and the level of humidity across the cities is dominated by synoptic scale weather variations. There are, however, caveats with this conclusion. First, there may be spatial gradient of absolute humidity from the coast in the coastal cities (Miami; Los Angeles, California) that we cannot detect given the sampling in these cities, that is, there are no stations within 10 km of the coast, see Fig. 1. Second, the conclusion of weak humidity sources in cities may not apply to areas with regular irrigation. For example, the sensor that was removed from our analysis for Tucson shows RH spiking to 100%, from values around 40%-60%, between 0600 and 0800 LT on weekday mornings. This is likely due to irrigation, and during this morning period w increased from ~10 to over 14 g kg⁻¹, which is a much larger change than the among-sensor variations. Also, we have focused on intraurban variability and the conclusion of limited variation in w may not hold for urbanrural variations.

One consequence of the minimal change in humidity could be lower increases in humidity from green infrastructure interventions designed to reduce temperature. These interventions might be expected to increase absolute humidity and offset some heat reduction from cooler temperatures. The analysis of Baltimore data shows insignificant relationship between absolute humidity and vegetation (as diagnosed using NDVI) during the morning and although there is a positive relationship during the afternoon (i.e., increased humidity when more vegetation) the change in humidity, and impact on heat metrics, is small.

A more practical consequence is that the spatial variations in RH, VPD, HI, and Hx within these cities can be estimated from spatially distributed measurements (or a high-resolution map) of T combined with just a single measurement of the absolute humidity. For example, if the spatial-mean w is used together with summer-mean T at each site to estimate the summer-mean HI, the root-mean-square errors between estimated and real HI are less than 0.28F for morning values and between 0.28 and 0.88F for afternoon values. This has financial implications for monitoring urban heat, as sensors that only measure T cost much less than sensors measuring T and RH.

We note that the minor role of variability of absolute humidity does not necessarily carry over to temporal variations in heat. In the cities studied the standard deviation of day-to-day variations in w (at fixed time of day) is around 2–3 g kg⁻¹,

which is comparable to the standard deviation of T (~38-48C). This suggests, based on analysis in section 3 [e.g., Eq. (3)], that w and T will play comparable roles in the temporal variations in heat and VPD. Also, there is generally low to moderate day-to-day correlations between w and T, which further suggests that variations in both T and w need to be considered if examining the daily variation in heat indices. This conclusion is supported by preliminary analysis of the Baltimore data, which shows that assuming the time-mean absolute humidity to estimate RH and heat indices from temperature measurements results in large RMSEs of around 10%-15% for RH and 2\$-4\$F for HI. A more detailed analysis is required but it appears daily variations in absolute humidity play an important role in daily variation in heat within cities.

Adnowledgments. We thank Katie O'Meara, Clara Hickman, and Sophie Stoerkel; the Maryland Institute College of Art for the radiation shield design; Erik Jorgensen, Jasmin Gonzalez, Dillon Ponzo, and Celine Sze for help with Baltimore field work; and Cathy Zhang for making the maps in Fig. 1. This work was supported by funding to JHU researchers from the Baltimore City Department of Sustainability, a JHU Alliance for a Healthier World Grant, NOAA Grant NA21OAR4310147, and DOE Grant DE-SC0023217. Any use of trade, firm, or product names is for descriptive purposes only and does not imply endorsement by the U.S. government.

Data availability statement. The temperature and humidity data used are available online [https://doi.org/10.5281/zenodo. 7336263 (JHU network; Waugh et al. 2022), http://erams.com/s/nsR7qpFiEeqUsBhm2quqZg/Urban_Veg_Cooling (UCR), and https://doi.org/10.6073/pasta/c1322bd2fb3e6eac0749a83033d24ab6 (UWM; Schatz et al. 2021)].

REFERENCES

Alduchov, O. A., and R. E. Eskridge, 1996: Improved Magnus's form approximation of saturation vapor pressure. J. Appl Meteor., 35, 601–609, https://doi.org/10.1175/1520-0450(1996) 035<0601:IMFAOS>2.0.CO2.

Alonzo, M., M. E. Baker, Y. Gao, and V. Shandas, 2021: Spatial configuration and time of day impact the magnitude of urban tree canopy cooling. *Environ. Res. Lett.*, 16, 084028, https:// doi.org/10.1088/1748-9326/ac12f2.

Anderson, G. B., M. L. Bell, and R. D. Peng, 2013: Methods to calculate the heat index as an exposure metric in environmental health research. *Environ. Health Perspect.*, 121, 1111– 1119, https://doi.org/10.1289/ehp.1206273.

Błażejczyk, K., G. Jendritzky, P. Bröde, D. Fiala, G. Havenith, Y. Epstein, A. Psikuta, and B. Kampmann, 2013: An introduction to the universal thermal climate index (UTCI). Geogr. Pol., 86, 5–10, https://doi.org/10.7163/GPol.2013.1.

Budd, G. M., 2008: Wet-bulb globe temperature (WBGT)—Its history and its limitations. J. Sci. Med. Sport, 11, 20–32, https://doi.org/10.1016/j.jsams.2007.07.003.

Copernicus, 2023: Sentinel-2 LC-1 data. Accessed 30 August 2023, https://developers.google.com/earth-engine/datasets/catalog/ sentinel-2.

- Farquhar, G. D., and T. D. Sharkey, 1982: Stomatal conductance and photosynthesis. Annu. Rev. Plant Physiol., 33, 317–345, https://doi.org/10.1146/annurev.pp.33.060182.001533.
- Fenner, D., A. Holtmann, F. Meier, I. Langer, and D. Scherer, 2019: Contrasting changes of urban heat island intensity during hot weather episodes. *Environ. Res. Lett.*, 14, 124013, https://doi.org/ 10.1088/1748-9326/ab506b.
- Gosling, S. N., and Coauthors, 2014: A glossary for biometeorology. Int. J. Biometeor., 58, 277–308, https://doi.org/10.1007/s00484-013-0729-9.
- Grossiord, C., T. N. Buckley, L. A. Cernusak, K. A. Novick, B. Poulter, R. T. W. Siegwolf, J. S. Sperry, and N. G. McDowell, 2020: Plant responses to rising vapor pressure deficit. New Phytol., 226, 1550–1566, https://doi.org/10.1111/nph.16485.
- Hall, S. J., and Coauthors, 2016: Convergence of microclimate in residential landscapes across diverse cities in the United States. *Landscape Ecol.*, 31, 101–117, https://doi.org/10.1007/ s10980-015-0297-y.
- Hoffman, J. S., V. Shandas, and N. Pendleton, 2020: The effects of historical housing policies on resident exposure to intraurban heat: A study of 108 US urban areas. *Climate*, 8, 12, https://doi.org/10.3390/di8010012.
- Ibsen, P. C., and Coauthors, 2021: Greater aridity increases the magnitude of urban nighttime vegetation-derived air cooling. Environ. Res. Lett., 16, 034011, https://doi.org/10.1088/1748-9326/abdf8a.
- Lu, Y.-C., and D. M. Romps, 2022: Extending the heat index. J. Appl. Meteor. Climatol., 61, 1367–1383, https://doi.org/10. 1175/JAMC-D-22-0021.1.
- Novick, K. A., and Coauthors, 2016: The increasing importance of atmospheric demand for ecosystem water and carbon fluxes. Nat. Climate Change, 6, 1023–1027, https://doi.org/10.1038/ nclimate3114.
- Phiri, D., M. Simwanda, S. Salekin, V. R. Nyirenda, Y. Murayama, and M. Ranagalage, 2020: Sentinel-2 data for land cover/use mapping: A review. *Remote Sens.*, 12, 2291, https://doi.org/10.3390/rs12142291.
- Richard, Y., and Coauthors, 2021: Is urban heat island intensity higher during hot spells and heat waves (Dijon, France, 2014–2019)? *Urban Climate*, 35, 100747, https://doi.org/10. 1016/j.uclim.2020.100747.
- Saverino, K. C., E. Routman, T. R. Lookingbill, A. M. Eanes, J. S. Hoffman, and R. Bao, 2021: Thermal inequity in Richmond, VA: The effect of an unjust evolution of the urban landscape on urban heat islands. Sustainability, 13, 1511, https://doi.org/10.3390/su13031511.
- Schatz, J., and C. J. Kucharik, 2014: Seasonality of the urban heat island effect in Madison, Wisconsin. J. Appl. Meteor. Climatol., 53, 2371–2386, https://doi.org/10.1175/JAMC-D-14-0107.1.
- —, and —, 2015: Urban climate effects on extreme temperatures in Madison, Wisconsin, USA. Environ. Res. Lett., 10, 094024, https://doi.org/10.1088/1748-9326/10/9/094024.
- —, C. Ziter, and C. Kucharik, 2021: WSC—Temperature and relative humidity data from 150 locations in and around Madison, Wisconsin from 2012–2020 ver 21. Environmental Data Initiative, accessed 30 September 2021, https://doi.org/ 10.6073/pasta/c1322bd2fb3e6eac0749a83033d24ab6.
- Scott, A. A., B. Zaitchik, D. W. Waugh, and K. O'Meara, 2017: Intraurban temperature variability in Baltimore. J. Appl. Meteor.

- Climatol., 56, 159–171, https://doi.org/10.1175/JAMC-D-16-0232.1.
- Seneviratne, S. I., and Coauthors, 2021: Weather and climate extreme events in a changing climate. Climate Change 2021: The Physical Science Basis, V. Masson-Delmotte et al., Eds., Cambridge University Press, 1513–1766, https://doi.org/10. 1017/9781009157896.013.
- Shandas, V., J. Voelkel, J. Williams, and J. Hoffman, 2019: Integrating satellite and ground measurements for predicting locations of extreme urban heat. Climate, 7, 5, https://doi.org/ 10.3390/cli7010005.
- Shi, R., B. F. Hobbs, B. F. Zaitchik, D. W. Waugh, A. A. Scott, and Y. Zhang, 2021: Monitoring intra-urban temperature with dense sensor networks: Fixed or mobile? An empirical study in Baltimore, MD. *Urban Climate*, 39, 100979, https:// doi.org/10.1016/j.uclim.2021.100979.
- Steadman, R. G., 1984: A universal scale of apparent temperature.
 J. Climate Appl. Meteor., 23, 1674–1687, https://doi.org/10.1175/1520-0450(1984)023<1674:AUSOAT>2.0.CO;2.
- Taleghani, M., D. Sailor, and G. A. Ban-Weiss, 2016: Micrometeorological simulations to predict the impacts of heat mitigation strategies on pedestrian thermal comfort in a Los Angeles neighborhood. *Environ. Res. Lett.*, 11, 024003, https://doi.org/10.1088/1748-9326/11/2/024003.
- Terando, A. J., E. Youngsteadt, E. K. Meineke, and S. G. Prado, 2017: Ad hoc instrumentation methods in ecological studies produce highly biased temperature measurements. *Ecol Evol.*, 7, 9890–9904, https://doi.org/10.1002/ecc3.3499.
- Tuholske, C., K. Caylor, C. Funk, A. Verdin, S. Sweeney, K. Grace, P. Peterson, and T. Evans, 2021: Global urban population exposure to extreme heat. *Proc. Natl. Acad. Sci. USA*, 118, e2024792118, https://doi.org/10.1073/pnas.2024792118.
- Waugh, D. W., B. Zaitchik, and A. A. Scott, 2022: JHU Baltimore iButton data. Zenodo, accessed 19 November 2022, https:// doi.org/10.5281/zenodo.7336263.
- Yang, P., G. Ren, and W. Liu, 2013: Spatial and temporal characteristics of Beijing urban heat island intensity. J. Appl. Meteor. Climatol., 52, 1803–1816, https://doi.org/10.1175/JAMC-D-12-0125.1.
- —, and W. Hou, 2017: Temporal-spatial patterns of relative humidity and the urban dryness island effect in Beijing City. J. Appl. Meteor. Climatol., 56, 2221–2237, https://doi.org/10.1175/JAMC-D-16-0338.1.
- Zaitchik, B. F., K. O'Meara, K. Baja, A. A. Scott, D. W. Waugh, and M. C. McCormack, 2016: B'more cool: Monitoring the urban heat island at high density for health and urban design. Earthzine, https://earthzine.org/bmore-cool-monitoring-theurban-heat-island-at-high-density-for-health-and-urban-design/.
- Zipper, S. C., J. Schatz, C. J. Kucharik, and S. P. Loheide II, 2017: Urban heat island induced increases in evapotranspirative demand. *Geophys. Res. Lett.*, 44, 873–881, https://doi.org/10. 1002/2016GL072190.
- Ziter, C. D., E. J. Pedersen, C. J. Kucharik, and M. G. Turner, 2019: Scale-dependent interactions between tree canopy cover and impervious surfaces reduce daytime urban heat during summer. *Proc. Natl. Acad. Sci. USA*, 116, 7575–7580, https://doi.org/10.1073/pnas.1817561116.

Copyright of Journal of Applied Meteorology & Climatology is the property of American Meteorological Society and its content may not be copied or emailed to multiple sites or posted to a listserv without the copyright holder's express written permission. However, users may print, download, or email articles for individual use.